Agricultural and Forest Meteorology 149 (2009) 1820–1828

Contents lists available at ScienceDirect

Agricultural and Forest Meteorology

journal homepage: www.elsevier.com/locate/agrformet

Tidal effects on net ecosystem exchange of carbon in an estuarine wetland

Haiqiang Guo [a,c], Asko Noormets [b], Bin Zhao [a,*], Jiquan Chen [a,c], Ge Sun [b], Yongjian Gu [a], Bo Li [a], Jiakuan Chen [a]

[a] Ministry of Education Key Laboratory for Biodiversity Science and Ecological Engineering, Fudan University, Shanghai, China
[b] Southern Global Change Program, USDA Forest Service, Raleigh, NC, USA
[c] Department of Environmental Sciences, University of Toledo, Toledo, OH, USA

ARTICLE INFO

Keywords:
Estuarine wetland
Carbon flux
Tidal elevation
Eddy covariance
Spectral analysis
Respiration

ABSTRACT

One year of continuous data from two eddy-flux towers established along an elevation gradient in coastal Shanghai was analyzed to evaluate the tidal effect on carbon flux (F_c) over an estuarine wetland. The measured wavelet spectra and cospectra of F_c and other environmental factors demonstrated that the dynamics of F_c at both sites exhibited a tidal-driven pattern with obvious characteristics at scales between 10 and 20 days (256–512-h). Environmental factors exerted major controls on the carbon balance at finer temporal scales. F_c was more sensitive to tides at the low-elevation site than at the high-elevation site. Overall, the mean nighttime F_c during spring tides was lower than that during neap tides, indicating suppressed ecosystem respiration under inundation. Larger differences were observed at the low-elevation site due to longer inundation durations. In contrast, daytime F_c was more variable since plants reacted differently in different growth periods and under different tidal elevations. The amplitudes of diurnal F_c during tidal periods were larger than those reported for other wetland types, implying a great potential for future carbon sequestration. Whilst tides would also transport organic matter to nearby estuaries and hence may incur carbon emission in the receiving ecosystems. Thus, further study on lateral carbon transport is required to investigate the tidal effect on the carbon sink/source role of the wetland.

1. Introduction

Increased atmospheric concentrations of carbon dioxide (CO_2) and methane (CH_4) have stimulated great interest in studying the carbon exchange between terrestrial ecosystems and the atmosphere. However, coastal wetlands, especially salt marshes, have not been well-investigated in spite of their high net primary productivity (Howes et al., 1985) and high carbon sequestration strengths in the soils (Chmura et al., 2003). Furthermore, coastal wetlands worldwide are disappearing and degrading under pressure from development and land use change as well as the spread of invasive species (Zedler and Kercher, 2005).

Coastal wetlands are influenced by tides, which not only change the groundwater level but also water chemical properties such as pH, redox potential and nutrient content (Armstrong et al., 1985; Pennings and Callaway, 1992). These effects are likely to influence ecosystem processes and functions. For example, it is known that water availability exerts great effect on the decomposition of soil carbon (Chapin et al., 2002) and thus controls soil respiration (i.e., carbon loss to the atmosphere). Excess water constitutes a direct barrier to gas diffusion and suppresses soil respiration (Heinsch et al., 2004) and indirect regulations on carbon assimilation by plants (McHugh and Dighton, 2004; Wang et al., 2006). On a broad scale, tidal elevation largely accounts for the striking plant zonation found in most salt marshes (Bertness and Pennings, 2000). Tides also play an important role in lateral matter exchange, such as the import of inorganic nutrients into marshes and the export of organic nutrients from marshes, which in turn nourish the oceanic food chains (Teal and Howes, 2000). However, current knowledge of the tide-induced regulation of carbon fluxes in coastal wetlands remains limited, which also impedes forecasting how these systems may respond to climate change.

In this paper, we evaluated the tidal effect on the estuarine ecosystem carbon exchange by analyzing continuous carbon flux (F_c) data collected for one year from two sets of tower-based eddy covariance systems installed in different tide-affected areas. We hypothesized that carbon flux in the two areas would change as a function of the tidal phase and height because tidal influences would decrease with increasing distance from the sea and the accompanying elevation change. Consequently, differences in F_c between the two sites would be determined by differences in the

* Corresponding author. Tel.: +86 21 65642263; fax: +86 21 65642468.
E-mail address: zhaobin@fudan.edu.cn (B. Zhao).

0168-1923/$ – see front matter © 2009 Elsevier B.V. All rights reserved.
doi:10.1016/j.agrformet.2009.06.010

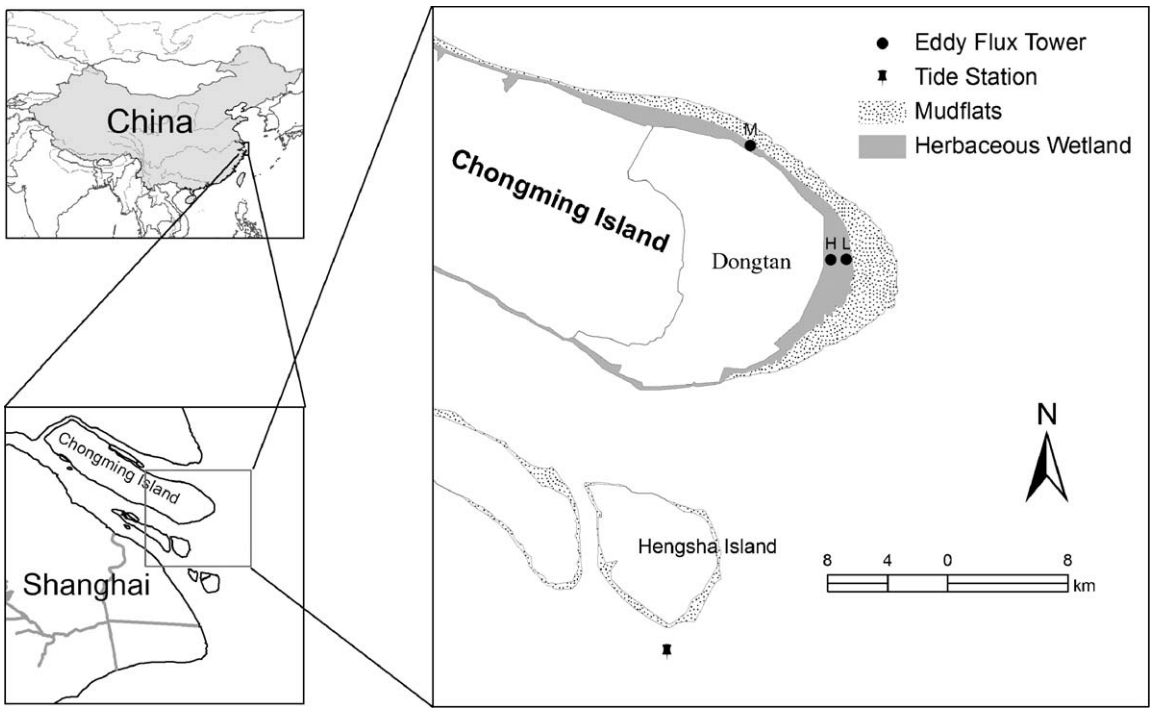

Fig. 1. Locations of Hengsha tidal station and the wetland study sites (H: high-elevation site; L: low-elevation site) at which eddy-flux towers were established.

suppression of respiration and alteration of photosynthesis due to tidal inundation.

2. Materials and methods

2.1. Study sites

Our study wetland lies on the easternmost side of Chongming Island in the estuary of the Yangtze River (31°25′–31°38′N, 121°50′–122°05′E) and has an area of 230 km^2 (Fig. 1). Due to the large amounts of sediment brought by the Yangtze River, the wetland continues to expand at a rate of 64 m per year toward the East China Sea (Zhao et al., 2008). Along the altitudinal gradient, fine particle in the soil increases with increasing nitrogen and organic matter content (Wu et al., 2005). The inclination of the tidal flat is normally <1% (Yang et al., 2002). The dominant plant species include *Phragmites australis* (hereafter, *Phragmites*), *Spartina alterniflora* (hereafter, *Spartina*) and *Scirpus mariqueter* (hereafter, *Scirpus*), which all form their respective monocultures. Compared to other two plants, *Scirpus* only accounts for a small portion of plant and ecosystem production. The climate of the area is characterized by strong seasonal variation and an abundance of precipitation. The annual precipitation in the study area was 1957–2192 mm in 2005 and the air temperature ranged from −5.2 °C to 36.5 °C, with an annual mean of 15.6 °C (see more details in Fig. 2).

Three eddy-flux towers were established on different elevations over the wetland in August of 2004 (Fig. 1). In this study, we used two of the three sites that are 1100 m apart and represent different elevation zones (0.5 m difference) and sensitivities to tidal activities. The site at the low elevation (L; 31°31.014′N, 121°58.300′E) is ca. 1600 m away from the sea wall constructed in 1998 and is dominated by *Phragmites*, *Spartina* and *Scirpus*. The site at the high elevation (H; 31°31.000′N, 121°57.643′E) is 500 m from the sea wall and dominated by *Phragmites* and *Spartina*. At

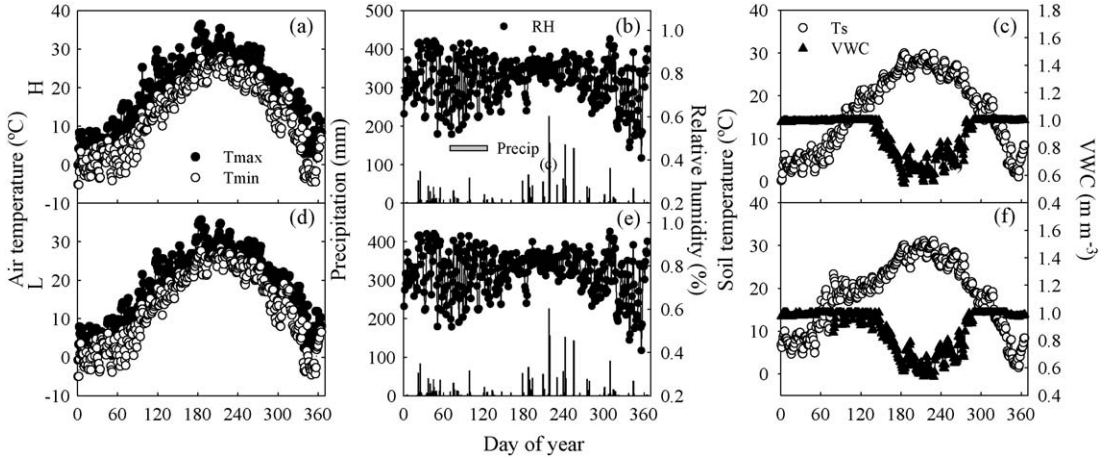

Fig. 2. Seasonal variations in major meteorological variables in 2005: (a and d) daily maximum and minimum air temperature (T_{max} and T_{min}); (b and e) daily total precipitation (Precip) and mean relative humidity (RH); and (c and f) daily averaged soil temperature (T_s) and soil volumetric water content (VWC). The figures above are for the high-elevation (H) site and the figures below are for the low-elevation (L) site.

Table 1
General characteristics of soil carbon content and salinity at the high- (H) and low- (L) elevation wetland study sites. Soil sample was obtained in early August, and the values were averaged for at least 30 samples at each depth for each site. The standard errors of the characters are given in parentheses.

Depth (cm)	Total carbon content (g C cm^{-3})		Salinity (‰)	
	H	L	H	L
0–10	0.019 (0.001)	0.016 (0.001)	3.8 (1.4)	4.6 (0.3)
10–20	0.018 (0.001)	0.016 (0.001)	4.6 (1.8)	3.3 (1.3)
20–30	0.016 (0.001)	0.015(0.001)	4.7 (1.4)	3.4 (1.1)
30–50	0.015 (0.001)	0.014 (0.001)	3.8 (1.0)	2.6 (0.9)
Average	0.017	0.015	4.2	3.5

site H, almost 95% of the source area was spontaneous plant, with an average leaf area index (LAI) of 5.14 m^2 m^{-2} in August. In contrast, approximately 70% of the source area was spontaneous plants, with 30% of bare ground and an average LAI of 2.58 m^2 m^{-2} at site L. The average carbon contents in the surface 0.5 m soils were 0.017 ± 0.001 (mean ± SE) and 0.015 ± 0.001 g C cm^{-3} at site H and L, respectively (Table 1). These values were in the range of but were lower than the mean value of carbon density in the salt marsh soils (0.039 ± 0.003 g C cm^{-3}, Chmura et al., 2003).

Tides in our study area are typically semidiurnal, with mean tidal ranges from 1.96 to 3.08 m (Sun et al., 2001) and maximum tidal ranges from 4.6 to 6.0 m above the Wusong Datum Plane (Yang et al., 2001). During the period of spring tides, most of the wetlands are inundated by seawater. Because of the lack of field records on tidal elevation during the study period, reference data were extracted from tide tables of the nearest tidal station (Hengsha station). Because the reference data were taken at 1-h intervals, interpolation procedures were used to obtain the tidal elevation for half-hour intervals, corresponding to our sites.

2.2. Flux system and meteorological instruments

F_c and sensible and latent heat were measured by the eddy covariance method with a three-axis sonic anemometer (CSAT-3, Campbell Scientific Inc., Logan, UT, USA) and open path infrared gas analyzer (IRGA, Li 7500, Li-Cor Inc., Lincoln, NE, USA), which were mounted 4.8 m above the ground at both sites. Some data gaps inevitably due to routine calibration of the Li7500 (from November 27th to December 9th, 2005).

Meteorological parameters were measured with an array of sensors. Net radiation was measured with a four component net radiometer (CNR1, Kipp and Zonen, Delft, Holland) positioned 4.5 m above the ground. Photosynthetically active radiation (PAR) was measured at 4 m above the ground using a Li190SB (Li-Cor Inc., Lincoln, NE, USA). Relative humidity and air temperature were measured with shielded sensors (HMP-45C, Vaisala, Helsinki, Finland) at heights of 1.6, 2.8 and 4.7 m at the higher-elevation site and at heights of 1.8, 2.5 and 4.8 m at the lower-elevation site. Rainfall was measured with a tipping bucket rain gauge (TE525, Texas Electronics, Texas, USA) mounted 4.5 m above the ground. Three replicates of soil temperature (0.05 m deep) were measured at each site using thermistors (model 107, CSI). Volumetric soil moisture was measured with a reflectometry sensor (CS616, CSI) at a depth of 0.05 m. Soil water potential was measured with soil moisture sensors (model 257, CSI) in two replicates at 0.05 m depth at each site. Thirty-minute averages were calculated for all micrometeorological measurements for use in further analyses.

2.3. Quality control of eddy covariance data

Turbulence fluxes were calculated as described by Saito et al. (2005) and implemented with EdiRe developed by the Institute of Atmospheric and Environmental Sciences, School of GeoSciences, The University of Edinburgh, England. Before calculating the fluxes of CO_2 and sensible and latent heat, wind velocity components were rotated so that the 30-min mean vertical and cross-wind components equated to zero. Corrections were made to rectify the influence of water vapor on the sonic temperature measurement (Kaimal and Gaynor, 1991), high frequency loss of signals due to equipment malfunction (Moore, 1986) and the effect of air density fluctuation on CO_2 and heat fluxes (Webb et al., 1980).

Other dispersed data gaps occurred due to rainfall events, dew or power failure. Stationary tests and integral turbulence tests were introduced to maintain quality control. During stationary tests, the procedure suggested by Foken and Wichura (1996) was applied, with the rejection threshold set to 30%. For the integral turbulence test, we utilized the tests for σ_w/u^* (Kaimal and Finnigan, 1994) and σ_c/c^* (Ohtaki, 1985), where u^* is the friction velocity, σ_w and σ_c are the 30-min standard deviations of vertical wind speed (w) and CO_2 density (c), respectively. c^* is defined as $c^* = -\overline{w'c'}/u^*$, where the over bar indicates a time average and the primes indicate fluctuations of the mean. The threshold values for rejecting σ_w/u^* and σ_c/c^* were set at 30% and 100% difference from the references, respectively.

As a result of the stationary test, about 25% and 33% of the F_c data was rejected for the high- and low-elevation sites, respectively, while about 2% and 6% of the data was rejected using the integral turbulence test. In total, about 29% and 41% of the F_c data was rejected for the sites H and L, respectively. By convention, positive values of F_c indicate a net loss of CO_2 to the atmosphere and the negative values indicate a net gain by the ecosystem.

2.4. Spectral analysis

To quantify the variability in F_c and the micrometeorological data caused by tidal cycles, the variance and covariance spectra were analyzed following the methods of Mallat (1989a, b), Meneveau (1991), Gamage and Blumen (1993), Qiu et al. (1995), Katul et al. (2001) and Stoy et al. (2005). The data was first normalized to zero mean and unit variance and was then transformed using orthonormal wavelet transformation (OWT), with a Haar function providing the basis for the temporal differencing characteristics and locality in the time domain (Mallat, 1989a, b). In the Haar transformation, the mother wavelet is defined as:

$$\varphi(x) = \begin{cases} 1, x \in \left[0, \frac{1}{2}\right) \\ -1, x \in \left(\frac{1}{2}, 1\right] \\ 0, \text{otherwise} \end{cases} \quad (1)$$

The basis functions are scaled and translated based on $\varphi(x)$, which can be processed across signals and hence transformed from a one-dimensional signal to a two-dimensional temporal representation. Though the spectral leakage inherent in orthonormal Haar functions (Meneveau, 1991; Gamage and Blumen, 1993; Qiu et al., 1995) was not examined in this paper, the large features of the spectral peaks reflecting diurnal and annual variability were hopefully resolved. The data gaps were padded with zero until 2^{14} data points were obtained, which represented 94% of the one-year data and covered 13 time scales from 0.5 to 4096 h (six months).

2.5. Light and temperature influences on F_c

The relationship between daytime F_c and PAR was estimated with the Landsberg Model (Chen et al., 2002):

$$F_c = P_{max} \times (1 - \exp(-\alpha \times (Q_{PAR} - I_{comp}))) \quad (2)$$

where P_{max} is the maximum rate of photosynthesis (μmol m^{-2} s^{-1}), α is apparent quantum yield, Q_{PAR} is PAR (μmol m^{-2} s^{-1}), and I_{comp} is the light compensation point.

For nighttime F_c, we followed the methods of Xu and Baldocchi (2004) to employ a model depicting the exponential relationship between nighttime F_c and soil temperature:

$$F_c = \beta_0 \times \exp(\beta_1 \times T_s) \quad (3)$$

where β_0 (μmol m^{-2} s^{-1}) is a scaling factor and β_1 is a parameter that represents the shape of the curve.

3. Results

3.1. Periodicity of F_c and the driving factors

The temporal changes and variations in F_c and other meteorological variables were characterized with clear diurnal and seasonal patterns (Fig. 3a and b). As expected, the normalized wavelet spectra of air temperature (T_a) and soil temperature (T_s) were similar across time scales. Net radiation (R_n) and PAR shared similar magnitudes of spectral energy. Generally, the wavelet spectra of solar radiation and temperature parameters varied in similar magnitudes at both sites over time. At both sites, F_c experienced a diurnal-scale peak and did not exhibit weekly spectral gaps, which was more obvious at site L. In our case, the tidal activities corresponded to lunar cycles with a periodicity of two weeks.

The cospectral analysis was conducted to inspect the relationships between meteorological variables and F_c and stronger correlations were observed at site H (Fig. 3c and d). We restricted the range of the normalized wavelet cospectrum to −0.3 to 0.2 in order to focus on the major driving factors at scales corresponding to the lunar cycle. For time scales of 10–20-d (256–512-h), tidal elevation (T_E) showed stronger negative correlations with F_c at site H than at site L. Both R_n and PAR were negatively correlated with F_c at the two sites but the correlations were stronger at site H. At both sites, R_n and PAR showed stronger negative correlations with F_c than T_E. The ratios of the wavelet cospectra between T_E and F_c to that between PAR and F_c were calculated to smooth the effects of the major factor (e.g., PAR) in 256–512-h scales. At the 256-h scale, a higher ratio was observed at site L (1.67 vs. 0.10 at site H), while at the 512-h scale, a slightly higher value was observed at site H (0.25 vs. 0.24 at site L), suggesting that tides exerted a greater effect on F_c of site L among the scales.

Interestingly, both T_a and T_s were negatively correlated with F_c at site H on the 256- and 512-h scales, whereas at site L, T_a was negatively correlated with F_c but T_s was positively correlated with F_c. The cospectral analysis of nighttime data showed that both T_a and T_s were positively correlated with F_c at both sites (not shown), which suggested that the response of daytime assimilation exceeded that of nighttime F_c and hence led to an overall negative relationship at site H; however, a stronger response of nighttime F_c led to a positive relationship at site L.

3.2. Tides and seasonal variation of F_c

During the growing season, the daily maximum F_c (i.e., daily maximum respiration) fluctuated at an interval of ~15 days, coinciding with the tidal period, and the periodicity was more obvious in site H than in site L. However, no obvious trends related to the tidal cycle were observed in the daily minimum F_c at either site (Fig. 4).

To better illustrate the tidal effect on the diurnal variations of F_c, the 4–5 days binned diurnal variation of F_c between spring and neap tides were presented (January, DOY 10–14 and DOY 16–20; April, DOY 114–118 and DOY 107–111; July, DOY 203–207 and DOY 195–198; October, DOY 289–293 and DOY 297–300; Fig. 5). In January, the differences between the two tidal phases were small at both sites and the amplitude of F_c was also small, fluctuating around zero. In April, the daytime C uptake was greater during spring tides than neap tides at both sites, with peak values reaching −7.0 and −12.0 μmol m^{-2} s^{-1} during spring tides at sites H and L, respectively, as compared to −3.8 and −3.3 μmol m^{-2} s^{-1} during neap tides. The greater effect at site L correlated well with the longer inundation durations. The effect of tidal phases in July was different from that in April, with larger differences of daytime F_c between spring and neap tides observed at site H. In October, the

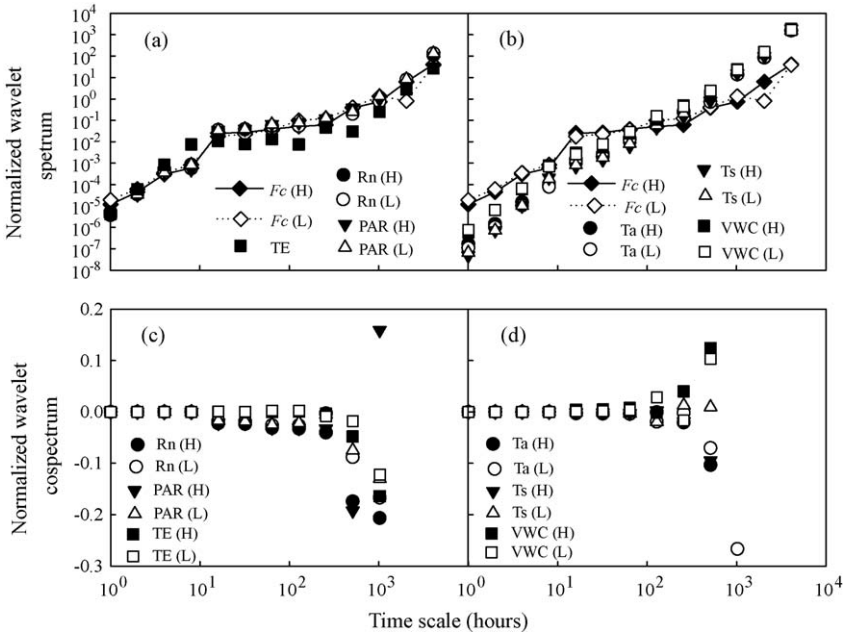

Fig. 3. Normalized wavelet spectra of CO_2 flux (F_c) and environmental drivers (a and b) and normalized wavelet cospectra between CO_2 flux (F_c) and environmental drivers (c and d) for the two wetland study sites (H: high-elevation site; L: low-elevation site). R_n: net radiation; PAR: photosynthetically active radiation; T_a: air temperature; T_s: soil temperature; VWC: volumetric water content of soil; T_E: tidal elevation.

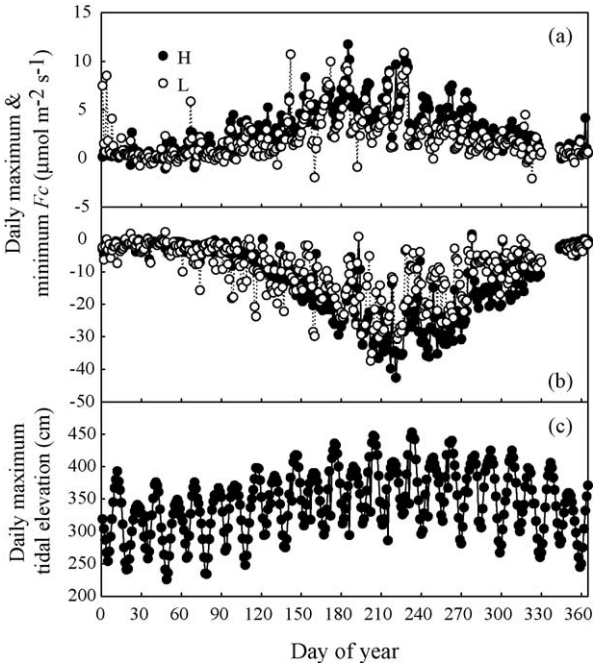

Fig. 4. Daily (a) maximum; (b) minimum CO_2 flux (F_c); and (c) daily maximum tidal elevation at the two wetland study sites in 2005 (H: high-elevation site; L: low-elevation site).

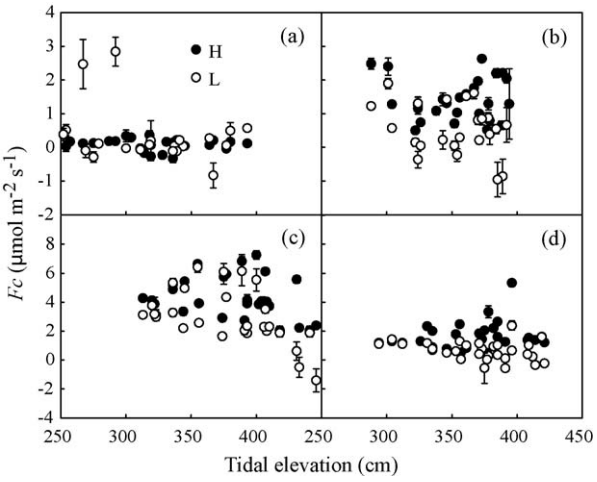

Fig. 6. Relationships between daily mean nighttime F_c and daily peak tidal elevation in: (a) January; (b) April; (c) July; and (d) October. Filled circles represent the high-elevation (H) site and open circles represent the low-elevation (L) site.

differences between the two tidal phases decreased but greater daytime uptake was observed during neap tides at site L. Since tidal phase was also associated with cardinal changes in wind direction, we compared the wind sectors associated with the tidal phases but did not detect consistent changes at either site.

Generally, lower nighttime emission was found during neap tides at both sites and a greater reduction was observed in site L, which could be explained by the higher water table and longer inundation duration during spring tides. However, no consistent relationships between daily mean nighttime F_c and daily peak tidal elevation was observed in April and July at either site; while nighttime mean F_c in January and October remained relatively steady (Fig. 6). The difference of the daytime F_c was more variable, which was the combined result of photosynthetic and respiratory processes.

3.3. Response of F_c to biophysical variables with tidal effects

The assimilation parameters P_{max} and alpha exhibited distinct responses to tidal phases (Fig. 7 and Table 2), whereas temperature explained little variability of nighttime F_c regardless of the tidal phase (Table 3). The ecosystem light response was evaluated from leaf emergence (April) to before plant senescence (October). Generally, PAR showed stronger correlations with F_c at site H, although the ranges of PAR differed throughout the three months. The peak values of P_{max} were observed in July at about −44 and −33 μmol m^{-2} s^{-1} for sites H and L, respectively. Alpha (α) was slightly greater at site L, although the differences were not always statistically significant and the compensation points (I_{comp}) were similar at both sites. In April and July, lower P_{max} (i.e., higher P_{max} value) was observed during spring tides, while lower P_{max} was observed during neap tides in October, which may reflect undermined photosynthetic capacity at site L.

Relationships between daytime F_c and PAR were simulated on a daily basis and the resulting I_{comp} exhibited different trends in the daily peak tidal elevation in different months (Fig. 8). Maximum T_E reached 450 cm in July and 420 cm in October but only 395 cm in April. For site H, in April, I_{comp} varied widely when T_E was less than

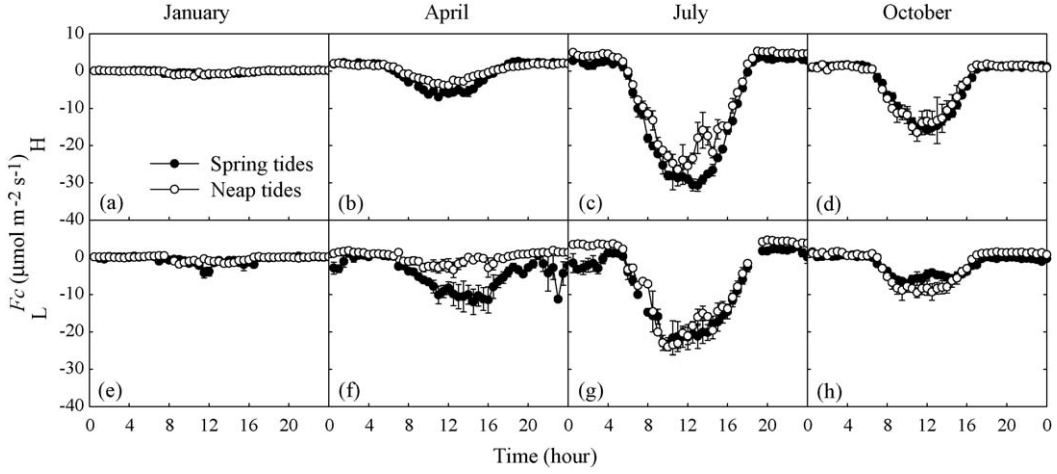

Fig. 5. Diurnal variations in CO_2 flux from 4 to 5 days in January (a and e), April (b and f), July (c and g) and October (d and h), 2005, for the two wetland study sites (H: high-elevation site, a–d; L: low-elevation site, e–h). Spring and neap tides, respectively, corresponded to: DOY 10–14 and DOY 16–20 (January); DOY 114–118 and DOY 107–111 (April); DOY 203–207 and DOY 195–198 (July); DOY 289–293 and DOY 297–300 (October). Error bars represent one standard error.

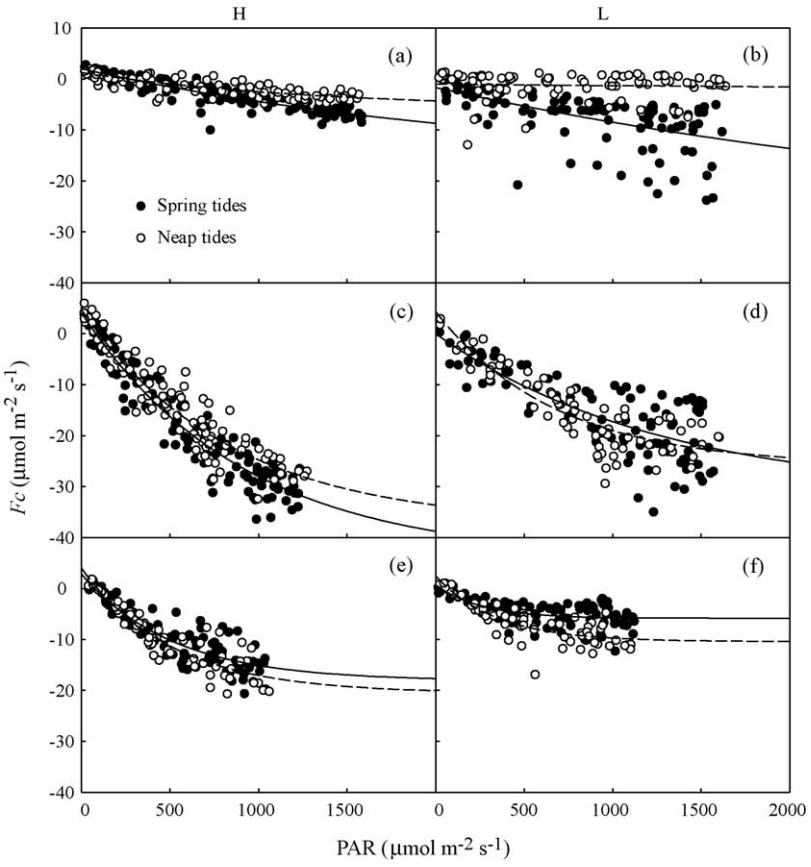

Fig. 7. Light response curves of CO_2 flux (F_c) based on the Landsberg Model for April (a and b), July (c and d) and October (e and f) for the two wetland study sites (H: high-elevation site; L: low-elevation site). The filled circles represent data from spring tides and the open circles represent data from neap tides.

Table 2
Parameters and R^2 values of the Landsberg Model (Eq. (2)) fitted to the daytime F_c data based on PAR at the two wetland study sites (H: high-elevation site; L: low-elevation site). Daytime F_c (μmol m^{-2} s^{-1}) is based on PAR (μmol m^{-2} s^{-1}). The parameters of the Landsberg Models (Eq. (2)) were fitted separately for six subsets of three months, April, July and October. For each month, 4–5 continuous clear days during spring and neap tides were selected separately.

Site	Month	DOY	Parameters (±standard error)			R^2
			P_{max}	α	I_{comp}	
H	April	114–118	−16.8 (7.5)*	0.0004 (0.0002)	273 (31)*	0.79
		107–111	−5.9 (2.2)*	0.0007 (0.0004)	259 (34)*	0.70
	July	203–207	−43.8 (4.4)*	0.0011 (0.0002)*	81 (15)*	0.91
		195–198	−37.5 (4.3)*	0.0012 (0.0002)*	99 (15)*	0.89
	October	289–293	−18.1 (2.0)*	0.0019 (0.0005)*	75 (20)*	0.79
		297–300	−20.6 (2.2)*	0.0020 (0.0004)*	91 (18)*	0.85
L	April	114–118	ns	ns	ns	0.32
		107–111	ns	ns	ns	0.00
	July	203–207	−32.9 (11.0)*	0.0007 (0.0004)	ns	0.60
		195–198	−25.9 (2.6)*	0.0015 (0.0003)*	106 (34)*	0.77
	October	289–293	−5.8 (0.4)*	0.0038 (0.0011)*	ns	0.36
		297–300	−10.4 (0.8)*	0.0029 (0.0006)*	73 (19)	0.73

* Statistically significant at $p < 0.05$ (t-test) and ns stands for no statistical significance. All models are significant at $p < 0.001$ (F-test).

350 cm; as T_E rose above 350 cm, I_{comp} decreased slightly. Certain levels of T_E seemed to act as barriers to soil respiration. At site H, in July, I_{comp} increased when T_E was less than 370 cm but then decreased quickly and remained relatively steady around 100 μmol m^{-2} s^{-1} as T_E rose above 390 cm. Interestingly, I_{comp} of site H varied considerably when T_E was between 370 and 390 cm. After carefully inspecting our data, we found that the points of high I_{comp} were from the day prior to flooding of the wetland and the points of low I_{comp} came from the day after flooding. I_{comp} at site L tended to decline with increasing T_E. In October, as soil moisture rose to 1.0, I_{comp} at both sites showed a slight increase with increasing T_E.

4. Discussion

In general, strong spectral peaks of meteorological variables and F_c occurred at a diurnal scale due to sunrise and sunset; broad spectral peaks were observed at a seasonal scale corresponding to changing weather conditions and plant phenology (Stoy et al., 2005). Previous studies have reported weekly or monthly spectral

Table 3
Parameters and R^2 values of nighttime F_c fitted to soil temperature (Eq. (3)) for the two wetland study sites (H: high-elevation site; L: low-elevation site). Nighttime F_c (μmol m^{-2} s^{-1}) is modeled (Eq. (3)) based on soil temperature at a depth of 0.05 m (°C).

Site	Month	DOY	Parameters (±standard error)		R^2
			β_0	β_1	
H	January	10–14	0.45 (0.16)*	−0.55 (0.17)*	0.12
		16–20	0.05 (0.03)	0.26 (0.12)*	0.08
	April	114–118	0.73 (0.19)*	0.06 (0.01)*	0.00
		107–111	0.32 (0.20)	0.10 (0.04)*	0.00
	July	203–207	0.12 (0.13)	0.11 (0.04)*	0.10
		195–198	0.13 (0.08)	0.13 (0.02)*	0.34
	October	289–293	3.22 (1.69)	−0.05 (0.03)	0.03
		297–300	0.20 (0.11)	0.11 (0.3)*	0.19
L	January	10–14	ns	ns	0.00
		16–20	1.01 (0.70)	−0.39 (0.15)*	0.12
	April	114–118	−0.03 (0.08)	0.21 (0.14)	0.05
		107–111	0.34 (0.37)	0.06 (0.05)	0.02
	July	203–207	ns	0.59 (0.26)*	0.16
		195–198	0.09 (0.05)	0.14 (0.02)*	0.43
	October	289–293	ns	ns	0.15
		297–300	0.24 (0.10)*	0.09 (0.02)*	0.22

* Statistically significant at $p < 0.05$ (t-test) and ns stands for no statistical significance.

gaps (Baldocchi et al., 2001; Stoy et al., 2005), but our data did not show such pattern at these scales, suggesting that F_c might be driven by factors such as weather fronts or ocean tides resulting from lunar cycles (Baldocchi, 1997; Baldocchi et al., 2001; Gu et al., 1999). Since no weather fronts at these scales were observed in our study, the tidal activities with a periodicity of two weeks could account for the missing weekly spectral gap. In other words, the dynamics of F_c at both sites exhibited a tidal-driven pattern with a temporal scale between 10- and 20-d (256–512-h). Nevertheless, environmental factors remained as the primary drivers for carbon balances at finer temporal scales at our study wetland. Because of the comparably lower plant cover, PAR, R_n and T_E showed weaker correlations with F_c at site L; however, the comparatively higher ratios of the cospectrum between T_E and F_c to that between PAR and F_c indicated that F_c was more sensitive to T_E during 256–512-h scales at that site, which supports our hypothesis that the degree of influence of tidal activities decreases with increasing distance from the sea.

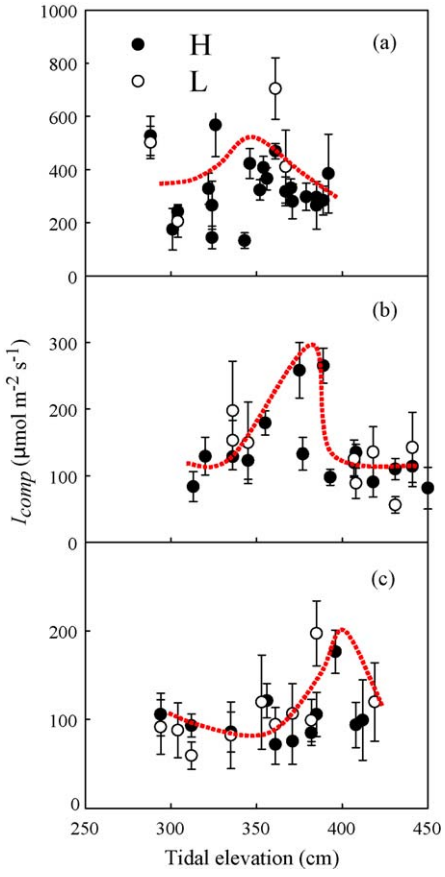

Fig. 8. The light compensation point (I_{comp}) derived on a daily basis from the Landsberg Model versus daily maximum tidal elevation in (a) April; (b) July; and (c) October. Filled circles represent the high-elevation (H) site and open circles represent the low-elevation (L) site. The dashed lines are trend lines.

Tidal effect should be largely explained by the suppression of CO_2 efflux from the soil as water creates a barrier against gas diffusion (Bouma and Bryla, 2000; Heinsch et al., 2004). Some compensation by aquatic biotic respiration could occur during inundation. The differences in nighttime F_c between spring and neap tides were greater at site L, which could be attributed to longer inundation durations due to the closer proximity to the sea. Concerning the photosynthesis capacity, both *Spartina* and *Phragmites*, especially *Spartina*, may benefit from some inundation. In general, *Spartina* favors high salinity with an optimum range around 15‰, while in contrast, *Phragmites* favors low salinity, suggesting high photosynthesis capacity during inundation (Wang et al., 2006). A similar phenomenon of increased photosynthetic activity during freshwater flooding has been reported on some low salinity-tolerant plants (Heilman et al., 1999; Heinsch et al., 2004). But here we have no direct evidence that *Phragmites* benefited from a reduction in salinity in the sediment during flooding.

At the beginning of the growing season (i.e., April), heterotrophic soil respiration may have contributed significantly to the daily F_c, so moderate inundation at this period led to higher ecosystem C uptake even though inundation may have also undermined the seedlings under the comparably low maximum tidal elevation (< 395 cm). During the peak growing season (i.e., July), higher carbon uptake rates were observed during spring tides at both sites; however, autotrophic respiration was high and plants showed strong resistance to inundation, leading to steady I_{comp} under high tidal elevation (Fig. 8). For example, *Spartina* has a well-developed system of aerenchyma, which functions as a conduit for gas exchange between the plant and the rhizosphere (Mendelssohn and Postek, 1982) and may allow autotrophic respiration to be independent of evapotranspiration. Preceding the senescent period (i.e., October), the differences of F_c between the two tidal phases became less. But interestingly, at site L, the values of daytime C uptake rates were larger during neap tides, indicating suppressed photosynthetic capacity under longer inundation periods (Landin, 1991; Mendelsohn and Mckee, 1988). This may also account for the small differences of daytime F_c in July. In most cases, larger amplitudes of mean diurnal F_c were observed during spring tides at both sites. These two areas of the estuarine wetland exhibited larger amplitudes of diurnal F_c when compared to other wetland types (Aurela et al., 2002; Glenn et al., 2006; Lafleur et al., 1997; Lafleur et al., 2001; Lafleur et al., 2003; Neumann et al., 1994; Syed et al., 2006). For example, an amplitude of about −8 to 4 μmol m^{-2} s^{-1} was observed in a coastal wetland (Heilman et al., 1999), and a slightly larger amplitude of about −12 to 4 μmol m^{-2} s^{-1} was observed in the same area (Heinsch et al., 2004). In their study, the wetland ecosystem was less productive, with low LAI (0.36 m^2 m^{-2}). In comparison, the seasonal averaged LAI of *Spartina* and *Phragmites* communities in Jiuduansha area, an island with a distance of ca. 35 km from our study area, were 4.4 and 2.1 m^2 m^{-2}, respectively. The mean seasonal net photosynthesis rates reached −24.4 and −16.3 μmol m^{-2} s^{-1} on leaf scale

(Liao et al., 2007). Moreover, comparing with the primary production measurement of *Spartina* and *Phragmites* communities in Jiuduansha area by Liao et al. (2007), the high amplitudes of F_c found in this study were comparable. Further, maximum C uptake rates were observed in July, about -26.4 μmol m^{-2} s^{-1} (site H) and -24.0 μmol m^{-2} s^{-1} (site L) during neap tides, and -30.6 μmol m^{-2} s^{-1} (site H) and -23.3 μmol m^{-2} s^{-1} (site L) during spring tides, respectively. These values were substantially higher than that measured at leaf scale, which showed P_{max} values of -30 and -28 μmol m^{-2} s^{-1} for *Spartina* and *Phragmites*, with LAI of 7 and 5 m^2 m^{-2}, respectively (Jiang, 2006). Even when taking into account the soil respiration rates of ~1 μmol m^{-2} s^{-1} (*Spartina* community) and ~7 μmol m^{-2} s^{-1} (*Phragmites* community) in the same study, our results remained higher than that of Jiang (2006). The nighttime respiration rates fluctuated around 1–4 μmol m^{-2} s^{-1} during spring tides at both sites, with values slightly higher during neap tides, suggesting that wetland ecosystems could act as strong C sinks with typical respiration rates and surprisingly high carbon uptake capacity, especially during spring tides.

The fact that tidal activities reduced ecosystem CO_2 emission, especially during the growing season, indicates that these coastal wetlands could act as strong C sinks. However, it should be noted that, unlike other non-tidal affected wetlands, coastal wetlands could laterally transport their redundant organic carbon to remote estuaries or open ocean by tides (Chalmers et al., 1985; Odum et al., 1979; Teal, 1962; Turner et al., 1979; Valiela et al., 2000). This means the role of coastal wetlands as C sink could be undermined since the transported carbon may also be emitted as CO_2 to atmosphere in the receiving ecosystems. Regrettably, scientists have not obtained a consistent conclusion on the percentage of carbon transported by tides so far. For the *Spartina* marsh, the exported total organic carbon accounted for 19–63% of the net aerial primary production of the marsh (Axelrad et al., 1976; Dame et al., 1991; Roman and Daiber, 1989; Williams et al., 1992). Generally, *Spartina* marsh on low tideland exported more carbon than that on high tideland (Taylor and Allanson, 1995). Odum (2000) reported that the extent of carbon export depends on the productivity and marsh coverage within the estuary and the tidal amplitude and the geomorphology of estuarine landscape. In addition, storms and high spring tides often incur large exports (Odum, 2000; Roman and Daiber, 1989). The tidal-induced lateral transports of carbon tend to be more site-specific and more work is required to quantify the carbon export in this study.

5. Conclusions

Using the eddy covariance method, we measured carbon fluxes of two estuarine wetlands and their relationships to tidal activities. We conclude that tides have substantial effects on carbon sequestration in wetlands, although solar and temperature factors exert major controls on the carbon balance at finer temporal scales (<days). Larger differences of nighttime F_c between spring and neap tides were recorded at the low-elevation site due to closer distance to the sea and hence longer inundation durations. However, the decreased nighttime F_c did not directly indicate declining respiratory activity in the sediments during inundation periods, rather than CO_2 emission. The photosynthetic responses to tidal activity were more complicated, as tidal flooding in July exerted positive or moderate effect on the photosynthetic activity at the high-elevation site, but hampered photosynthetic activity at the low-elevation site. However, an opposite phenomenon recorded in April indicated that great attention should be paid when evaluating the potential effect of sea level rising on the carbon cycling of wetland ecosystems.

Acknowledgements

This research was supported by the National Basic Research Program of China (no. 2006CB403305), the National Natural Science Foundation of China (no. 40471087), Shanghai Municipal Natural Science Foundation (no. 06ZR14015) and the Program for New Century Excellent Talents in University (NCET-06-0364) funded by the Ministry of Education of China. We also appreciate all the dedicated help from US-China Carbon Consortium (USCCC). We thank all of the staff of the Shanghai Chongming Dongtan National Nature Reserve and all of the students in our laboratory for their help with carbon flux tower construction, laboratory and field work and comments on the manuscript. Thanks are extended to Paul C. Stoy, Wen Xuefa, Jiang Zhaoyang, Cheng Weixin, Kim Brosofske, Lisa Delp, Osbert Sun and two anonymous referees for their expert advice and fruitful comments.

References

Armstrong, W., Wright, E.J., Lythe, S., Gaynard, T.J., 1985. Plant zonation and the effects of the spring-neap tidal cycle on soil aeration in a humber salt marsh. J. Ecol. 73 (1), 323–339.

Aurela, M., Laurila, T., Tuovinen, J.P., 2002. Annual CO_2 balance of a subarctic fen in northern Europe: importance of the wintertime efflux. J. Geophys. Res. Atmos. 107 (D21).

Axelrad, D.M., Moore, K.A., Bender, M.E., 1976. Nitrogen, phosphorus and carbon flux in Chesapeake Bay marshes. Virginia Water Resour. Res. Center Bull. 79, 182.

Baldocchi, D., 1997. Measuring and modelling carbon dioxide and water vapour exchange over a temperate broad-leaved forest during the 1995 summer drought. Plant Cell Environ. 20 (9), 1108–1122.

Baldocchi, D., Falge, E., Wilson, K., 2001. A spectral analysis of biosphere-atmosphere trace gas flux densities and meteorological variables across hour to multi-year time scales. Agric. For. Meteorol. 107 (1), 1–27.

Bertness, M.D., Pennings, S.C., 2000. Spatial variation in process and pattern in salt marsh plant communities in eastern North America. In: Weinstein, M.P., Kreeger, D.A. (Eds.), Concepts and Controversies in Tidal Marsh Ecology. Kluwer Academic Publishers, Dordrecht, pp. 39–58.

Bouma, T.J., Bryla, D.R., 2000. On the assessment of root and soil respiration for soils of different textures: interactions with soil moisture contents and soil CO_2 concentrations. Plant Soil 227 (1-2), 215–221.

Chalmers, A.G., Wiegert, R.G., Wolf, P.L., 1985. Carbon balance in a salt marsh: interactions of diffusive export, tidal deposition and rainfall-caused erosion. Estuar. Coast. Shelf Sci. 21, 757–771.

Chapin, F.S., Maston, P.A., Mooney, H.A., 2002. Principles of Terrestrial Ecosystem Ecology. Springer-Verlag, New York.

Chen, J.Q., Falk, M., Euskirchen, E., Paw, U.K.T., Suchanek, T.H., Ustin, S.L., Bond, B.J., Brosofske, K.D., Phillips, N., Bi, R.C., 2002. Biophysical controls of carbon flows in three successional Douglas-fir stands based on eddy-covariance measurements. Tree Physiol. 22 (2–3), 169–177.

Chmura, G.L., Anisfeld, S.C., Cahoon, D.R., Lynch, J.C., 2003. Global carbon sequestration in tidal, saline wetland soils. Glob. Biogeochem. Cycle 17 (4), 1111.

Dame, R.F., Spurrier, J.D., Williams, T.M., Kjerfve, R., Zingmark, R.G., Wolaver, T.G., Chrzanowski, T.H., McKellar, H.N., Vernberg, F.J., 1991. Annual material processing by a salt marsh-estuarine basin in South Carolina, USA. Mar. Ecol. Prog. Ser. 72, 153–166.

Foken, T., Wichura, B., 1996. Tools for quality assessment of surface-based flux measurements. Agric. For. Meteorol. 78 (1–2), 83–105.

Gamage, N., Blumen, W., 1993. Comparative analysis of low-level cold fronts: wavelet, Fourier, and empirical orthogonal function decompositions. Mon. Weather Rev. 121, 2867–2878.

Glenn, A.J., Flanagan, L.B., Syed, K.H., Carlson, P.J., 2006. Comparison of net ecosystem CO_2 exchange in two peatlands in western Canada with contrasting dominant vegetation, Sphagnum and Carex. Agric. For. Meteorol. 140 (1–4), 115–135.

Gu, L.H., Fuentes, J.D., Shugart, H.H., Staebler, R.M., Black, T.A., 1999. Responses of net ecosystem exchanges of carbon dioxide to changes in cloudiness: results from two North American deciduous forests. J. Geophys. Res. -Atmos. 104 (D24), 31421–31434.

Heilman, J.L., Cobos, D.R., Heinsch, F.A., Campbell, C.S., McInnes, K.J., 1999. Tower-based conditional sampling for measuring ecosystem-scale carbon dioxide exchange in coastal wetlands. Estuaries 22, 584–591.

Heinsch, F.A., Heilman, J.L., McInnes, K.J., Cobos, D.R., Zuberer, D.A., Roelke, D.L., 2004. Carbon dioxide exchange in a high marsh on the Texas Gulf Coast: effects of freshwater availability. Agric. For. Meteorol. 125 (1–2), 159–172.

Howes, B.L., Dacey, J.W.H., Teal, J.M., 1985. Annual carbon mineralization and belowground production of *Spartina alterniflora* in a New England salt marsh. Ecology 66 (2), 595–605.

Jiang, L.F., 2006. Effects of invasion of *Spartina alterniflora* on production processes of ecosystems in estuarine wetlands of the Yangtze River, China: a comparative study of invasive and native species. Postdoctoral Thesis, Fudan University.

Kaimal, J.C., Finnigan, J.J., 1994. Atmospheric Boundary Layer Flows. Oxford University Press, 289 pp.
Kaimal, J.C., Gaynor, J.E., 1991. Another look at sonic thermometry. Bound. -Layer Meteor. 56, 401–410.
Katul, G., Lai, C.T., Schafer, K., Vidakovic, B., Albertson, J., Ellsworth, D., Oren, R., 2001. Multiscale analysis of vegetation surface fluxes: from seconds to years. Adv. Water Resour. 24 (9–10), 1119–1132.
Lafleur, P.M., McCaughey, J.H., Joiner, D.W., Bartlett, P.A., Jelinski, D.E., 1997. Seasonal trends in energy, water, and carbon dioxide fluxes at a northern boreal wetland. J. Geophys. Res. -Atmos. 102 (D24), 29009–29020.
Lafleur, P.M., Roulet, N.T., Admiral, S.W., 2001. Annual cycle of CO_2 exchange at a bog peatland. J. Geophys. Res. -Atmos. 106 (D3), 3071–3081.
Lafleur, P.M., Roulet, N.T., Bubier, J.L., Frolking, S., Moore, T.R., 2003. Interannual variability in the peatland-atmosphere carbon dioxide exchange at an ombrotrophic bog. Glob. Biogeochem. Cycle 17 (2).
Landin, M.C., 1991. Growth habits and other considerations of smooth cordgrass, *Spartina alterniflora* Loisel. In: Mumford, T.F., Peyton, J.P., Sayce, J.R., Harbell, S. (Eds.), Spartina Workshop Record, Washington Sea Grant Program, University of Washington, Seattle, pp. 15–20.
Liao, C.Z., Luo, Y.Q., Jiang, L.F., Zhou, X.H., Wu, X.W., Fang, C.M., Chen, J.K., Li, B., 2007. Invasion of *Spartina alterniflora* enhanced ecosystem carbon and nitrogen stocks in the Yangtze Estuary, China. Ecosystems 10, 1351–1361.
Mallat, S., 1989a. A theory for multiresolution signal decomposition: the wavelet representation. IEEE Trans. Pattern Anal. Mach. Intell. 11, 674–693.
Mallat, S., 1989b. Multiresolution approximations and wavelet orthonormal bases of L^2 (R). Trans. Am. Math. Soc. 315, 69–87.
McHugh, J.M., Dighton, J., 2004. Influence of mycorrhizal, inoculation, inundation period, salinity, and phosphorus availability on the growth of two salt marsh grasses, *Spartina alterniflora* Lois. and *Spartina cynosur*oides (L.) Roth., in nursery systems. Restor. Ecol. 12 (4), 533–545.
Mendelsohn, I.A., Mckee, K.L., 1988. *Spartina alterniflora* die-back in Louisiana: time-course investigation of soil waterlogging effects. J. Ecol. 76, 509–521.
Mendelssohn, I.A., Postek, M.T., 1982. Elemental analysis of deposits on the roots of *Spartina alterniflora* Loisel. Am. J. Bot. 22, 904–912.
Meneveau, C., 1991. Analysis of turbulence in the orthonormal wavelet representation. J. Fluid Mech. 232, 469–620.
Moore, C.J., 1986. Frequency response corrections for eddy correlation systems. Bound. -Layer Meteor. 37, 17–35.
Neumann, H.H., Denhartog, G., King, K.M., Chipanshi, A.C., 1994. Carbon-dioxide fluxes over a raised open bog at the Kinosheo Lake tower site during the Northern Wetlands Study (NOWES). J. Geophys. Res. -Atmos. 99 (D1), 1529–1538.
Odum, W.E., Fisher, J.S., Pickrel, J.C., 1979. Factors controlling the flux of particulate organic carbon from estuarine wetlands. In: Livingston, R.J. (Ed.), Ecological Processes in Coastal and Marine Systems. Plenum Press, New York, pp. 69–79.
Odum, E.P., 2000. Tidal marshes as upwelling/pulsing systems. In: Weinstein, M.P., Kreeger, D.A. (Eds.), Concepts and Controversies in Tidal Marsh Ecology. Kluwer Academic Publishers, Dordrecht, pp. 3–7.
Ohtaki, E., 1985. On the similarity in atmospheric fluctuations of carbon dioxide, water vapor and temperature over vegetated fields. Bound. -Layer Meteor. 32, 25–37.
Pennings, S.C., Callaway, R.M., 1992. Salt-marsh plant zonation: the relative importance of competition and physical factors. Ecology 73 (2), 681–690.
Qiu, J., Paw, U.K.T., Shaw, R.H., 1995. The leakage problem of orthonormal wavelet transforms when applied to atmospheric turbulence. J. Geophys. Res. 100 (D12), 25,769–25,779.
Roman, C.T., Daiber, F.C., 1989. Organic carbon flux through a Delaware Bay salt marsh: tidal exchange, particle size distribution, and storms. Mar. Ecol. Prog. Ser. 54, 149–156.
Saito, M., Miyata, A., Nagai, H., Yamada, T., 2005. Seasonal variation of carbon dioxide exchange in rice paddy field in Japan. Agric. For. Meteorol. 135 (1–4), 93–109.
Stoy, P.C., Katul, G.G., Siqueira, M.B.S., Juang, J.Y., McCarthy, H.R., Kim, H.S., Oishi, A.C., Oren, R., 2005. Variability in net ecosystem exchange from hourly to inter-annual time scales at adjacent pine and hardwood forests: a wavelet analysis. Tree Physiol. 25 (7), 887–902.
Sun, S.C., Cai, Y.L., Liu, H., 2001. Biomass allocation of *Scirpus mariqueter* along an elevational gradient in a salt marsh of the Yangtse River estuary. Acta Bot. Sin. 43, 178–185.
Syed, K.H., Flanagan, L.B., Carlson, P.J., Glenn, A.J., Van Gaalen, K.E., 2006. Environmental control of net ecosystem CO_2 exchange in a treed, moderately rich fen in northern Alberta. Agric. For. Meteorol. 140 (1–4), 97–114.
Taylor, D.I., Allanson, B.R., 1995. Organic carbon fluxes between a high marsh and estuary, and the inapplicability of the outwelling hypothesis. Mar. Ecol. Prog. Ser. 120, 263–270.
Teal, J.M., 1962. Energy flow in the salt marsh ecosystem of Georgia. Ecology 43, 614–624.
Teal, J.M., Howes, B.L., 2000. Salt marsh values: retrospection from the end of the century. In: Weinstein, M.P., Kreeger, D.A. (Eds.), Concepts and Controversies in Tidal Marsh Ecology. Kluwer Academic Publishers, Dordrecht, pp. 9–18.
Turner, R.E.S., Woo, W., Jitts, H.R., 1979. Estuarine influences on a continental shelf plankton community. Science 206, 218–220.
Valiela, I., Cole, M.L.J.M., Hauxwell, J.J.C.S.B.J., 2000. Role of salt marshes as part of coastal landscape. In: Weinstein, M.P., Kreeger, D.A. (Eds.), Concepts and Controversies in Tidal Marsh Ecology. Kluwer Academic Publishers, Dordrecht, pp. 23–38.
Wang, Q., Wang, C.H., Zhao, B., Ma, Z.J., Luo, Y.Q., Chen, J.K., Li, B., 2006. Effects of growing conditions on the growth of and interactions between salt marsh plants: implications for invasibility of habitats. Biol. Invasions 8 (7), 1547–1560.
Webb, E.K., Pearman, G.I., Leuning, R., 1980. Correction of flux measurements for density effects due to heat and water vapor transfer. Q. J. R. Meteorol. Soc. 106, 85–100.
Williams, T.M., Wolaver, T.G., Dame, R.F., Spurrier, J.D., 1992. The Bly Creek ecosystem study-organic carbon transport within a euhaline salt marsh basin, North Inlet, South Carolina. J. Exp. Mar. Biol. Ecol. 163, 125–139.
Wu, J.H., Fu, C.Z., Lu, F., Chen, J.K., 2005. Changes in free-living nematode community structure in relation to progressive land reclamation at an intertidal marsh. Appl. Soil Ecol. 29 (1), 47–58.
Xu, L.K., Baldocchi, D.D., 2004. Seasonal variation in carbon dioxide exchange over a Mediterranean annual grassland in California. Agric. For. Meteorol. 123 (1–2), 79–96.
Yang, S.L., Ding, P.X., Chen, S.L., 2001. Changes in progradation rate of the tidal flats at the mouth of the Changjiang (Yangtze) River, China. Geomorphology 38 (1-2), 167–180.
Yang, S.L., Zhao, Q.Y., Ding, P.X., Zhu, J., 2002. Annual changes in coastal dynamic and SSC progresses as well as their statistic relationships to intertidal bed-level: Shanghai coast. Mar. Sci. 26, 37–41.
Zedler, J.B., Kercher, S., 2005. Wetland resources: status, trends, ecosystem services, and restorability. Annu. Rev. Environ. Resour. 30, 39–74.
Zhao, B., Guo, H.Q., Yan, Y.E., Wang, Q., Li, B., 2008. A simple waterline approach for tidelands using multi-temporal satellite images: a case study in the Yangtze Delta. Estuar. Coast. Shelf Sci. 77, 134–142.